Atomic-Scale Magnetometry of Dynamic Magnetization

J. van Bree and M. E. Flatté

Phys. Rev. Lett. **118**, 087601 — Published 23 February 2017

DOI: 10.1103/PhysRevLett.118.087601

Atomic-scale magnetometry of dynamic magnetization

J. van Bree* and M. E. Flatté†
Department of Physics and Astronomy and Optical Science and Technology Center, University of Iowa, Iowa City, Iowa 52242, USA
(Dated: January 9, 2017)

The spatial resolution of imaging magnetometers has benefitted from scanning probe techniques. The requirement that the sample perturbs the scanning probe through a magnetic field external to its volume limits magnetometry to samples with static moments. We propose a magnetometer in which the perturbation is reversed; the probe's magnetic field generates a response of the sample, which acts back on the probe and changes its energy. For an NV^- spin center in diamond this perturbation changes the fine structure splitting of the spin ground state. Sensitive measurement techniques using coherent detection schemes then permit detection of the magnetic response of paramagnetic and diamagnetic materials. This technique can measure the thickness of magnetically dead layers with better than 0.1 Å accuracy.

PACS numbers: 76.30.Mi,75.75.-c,85.75.-d,07.55.Jg

Imaging of magnetic moments and magnetic fields advances a wide range of fields: nuclear magnetic resonance [1] clarifies the structure of molecules and biological enzymes, SQUID magnetometry [2] characterizes magnetically engineered multilayers, and magnetic resonance imaging (MRI) [3] distinguishes various types of tissue in medicine and biology. The spatial resolution of imaging magnetometers suffices, in principle, to observe interesting processes, such as biological activity in a cell, which are obscured from optical measurements by the diffraction limit [4]. In practice, however, the spatial resolution of even specialized MRI rarely surpasses μm [5], limited by the sensitivity at which the nuclear spins can be detected [6]. Various scanning probe techniques [7–9] improve this spatial resolution. A promising approach, NV^--center magnetometry [10], uses a defect formed by a substitutional nitrogen atom and adjacent vacancy site in a diamond crystal. The long spin coherence time of this defect allows optical initialization and detection, and coherent manipulation with microwaves [11, 12], resulting in exceptional magnetic field sensitivity and spatial resolution at ambient conditions [4, 13]. These scanning probe based magnetometers require the sample's magnetic field to perturb the magnetically sensitive probe nearby. In NV^--center based magnetometry, for example, measurements of the splitting between the spin ground state $|J_z = \pm 1\rangle$ states detect this magnetic field, see Fig. 1(a). This scheme, however, requires the sample to possess an substantial magnetic field external to its volume, which excludes weak-moment films, as well as paramagnetic and diamagnetic materials, which lack such external magnetic fields in isolation.

Here we propose to overcome this disadvantage, by using the probe's magnetic field to perturb the sample instead of relying on the sample's magnetic field to perturb the probe. For any sample magnetic permeability differing from that of vacuum, the magnetic field of the probe will be dynamically altered, changing the magnetic energy stored in the probe's magnetic field. For this approach, depicted in Fig. 1(b), we predict that for a NV^--center these changes in magnetic energy effectively translate into a modification of the crystal field splitting of the NV^--center's spin ground state, see Fig. 1(a). Techniques have already been developed to measure small changes in this splitting for thermometry purposes [14–16]. Our calculations show that the magnetic energy approach to NV^--center magnetometry makes it possible to measure the magnetic permeabilities of diamagnetic and paramagnetic materials. For a unique application of this technique, we propose measuring the thickness of the magnetically dead layers [17]. We show it is possible to determine this thickness with an accuracy superior to 0.1 Å for experimentally realistic conditions.

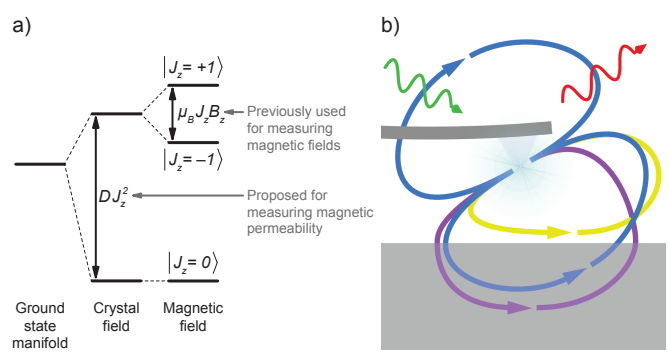

FIG. 1. (a) The NV^--center's ground state spin $J = 1$ is split by the crystal field and magnetic field. Conventional NV magnetometry utilizes the splitting of the $|J_z = \pm 1\rangle$ states. We propose a way to measure magnetic response of materials using the splitting between the $|J_z = 0\rangle$ and $|J_z = \pm 1\rangle$ states. (b) Implementation of magnetic-energy magnetometry. The spin of an NV^--center is located at the apex of a scanning probe tip, optically initialized (green) and detected (red). The spin's magnetic induction (blue) is perturbed by the presence of the sample (gray), leading to modifications of the magnetic induction (diamagnetic, yellow; paramagnetic, purple).

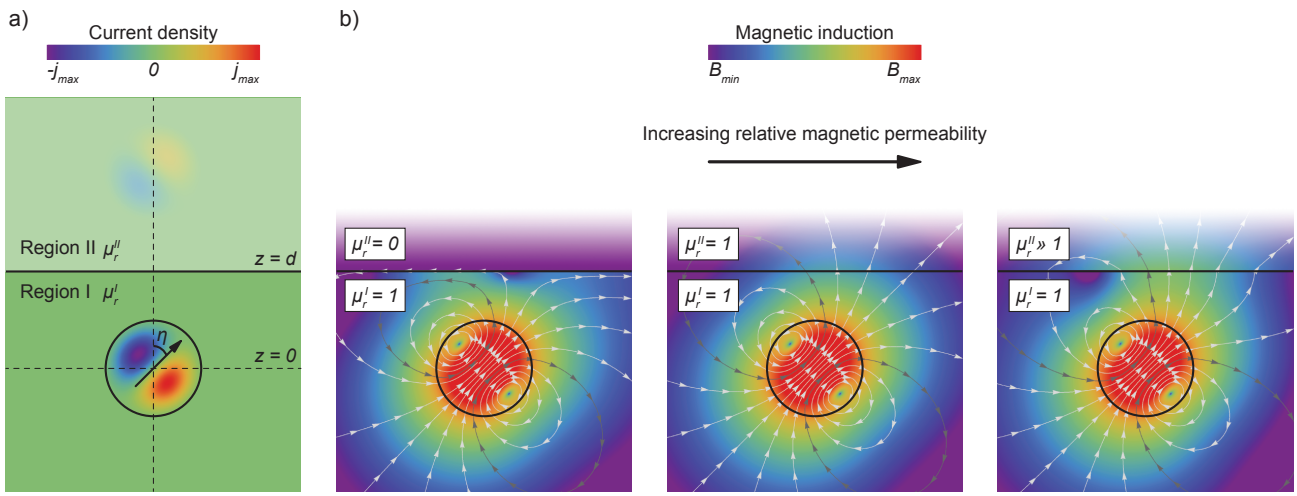

FIG. 2. (a) A spin is placed in region I with relative magnetic permeability μ_r^{I}, adjacent to a semi-infinite region II with μ_r^{II}, filling half-space $z > d$. The spin makes an angle η with respect to the normal of the interface between the two regions. The color indicates the magnitude of the (image) current distribution for $\mathcal{P}(r) = [j_0(\pi r/R)]^2$, a spherical Bessel function of zeroth order, and $\mu_r^{\mathrm{II}} = 2$. (b) The calculated magnetic induction for the situation as described in (a). The magnetic induction near the interface is parallel to the interface for diamagnetic substances ($\mu_r^{\mathrm{II}} = 0$, left), though perpendicular to the interface for paramagnetic materials ($\mu_r^{\mathrm{II}} \gg 1$, right). The magnitude of the magnetic induction is indicated by color, its direction by the arrows of the streamlines.

Consider a spin with total angular momentum J in region I, placed in close proximity to region II with a different magnetic permeability μ_r. In absence of spin-orbit coupling, its magnetic moment density

$$\langle \boldsymbol{\mu}(\mathbf{x}) \rangle = \frac{2\mu_B}{\hbar} \langle \mathbf{J}(\mathbf{x}) \rangle = \frac{2\mu_B}{\hbar} \langle \mathbf{J} \rangle \mathcal{P}(\mathbf{x}), \tag{1}$$

depends on its probability density $\mathcal{P}(\mathbf{x})$, and the expectation value of the spin operator $\mathbf{J} = (J_x, J_y, J_z)$; here μ_B is the Bohr magneton, and we took the g-factor to be 2. In the Supplemental Material [18] we show that this relation holds for any N-particle state, e.g. the complicated ground state of the NV$^-$-center comprising 6 electrons [19]. To simplify the calculation, we now treat the interaction of the spin's magnetic moment with its environment classically; we will address its quantum-mechanical nature later on. The presence of a magnetic moment density requires a current density $\mathbf{j}(\mathbf{x}) = \nabla \times \langle \boldsymbol{\mu}(\mathbf{x}) \rangle$, which provides a direct expression for calculating, in the Coulomb gauge, the energy stored in a magnetic field [20],

$$E_{\mathrm{mag}} = \frac{1}{2} \int \mathbf{j}(\mathbf{x}) \cdot \mathbf{A}(\mathbf{x}) \, d^3x. \tag{2}$$

Here $\mathbf{A}(\mathbf{x})$ is the vector potential produced by $\mathbf{j}(\mathbf{x})$. If $\mathbf{j}(\mathbf{x}) = 0$ in region II, Eq. 2 determines the magnetic energy from $\mathbf{A}(\mathbf{x})$ in region I alone. The effect of region II on the spin's vector potential in region I can be included by replacing region II with an image current density [20]

$$\widetilde{\mathbf{j}}(\mathbf{x}) = \frac{\mu_r^{\mathrm{II}} - \mu_r^{\mathrm{I}}}{\mu_r^{\mathrm{II}} + \mu_r^{\mathrm{I}}} \begin{pmatrix} j_x(x, y, 2d - z) \\ j_y(x, y, 2d - z) \\ -j_z(x, y, 2d - z) \end{pmatrix}_{\hat{\mathbf{x}}, \hat{\mathbf{y}}, \hat{\mathbf{z}}}, \tag{3}$$

where for simplicity we neglect any surface current at the interface between the regions. A treatment of surface currents would be required for conductive materials with a non-zero component of their magnetization parallel to the surface normal at the interface of the two regions. The image current generates a vector potential $\widetilde{\mathbf{A}}(\mathbf{x})$; the total vector potential in region I is then $\mathbf{A}(\mathbf{x}) + \widetilde{\mathbf{A}}(\mathbf{x})$.

For ease of calculation we assume isolated spin systems are approximately spherically symmetric and limited to a sphere with radius $R < d$. We will show later on that is a fair approximation for the NV$^-$-center, even though that spin center has C_{3v}-symmetry [19]. For a spin oriented such that its integrated magnetic moment makes an angle η with respect to the z-axis (see Fig. 2(a)), the spin's current density

$$\mathbf{j}(\mathbf{x}) = 2\mu_B J \frac{d\mathcal{P}(r)}{dr} \times \begin{pmatrix} 0 \\ \sin\eta \sin\phi \\ \sin\eta \cos\theta \cos\phi - \cos\eta \sin\theta \end{pmatrix}_{\hat{\mathbf{r}}, \hat{\boldsymbol{\theta}}, \hat{\boldsymbol{\phi}}}, \tag{4}$$

for $r \leq R$. The vector potential resulting from this current distribution, calculated by expanding the Green's function in spherical harmonics and performing several (partial) integrations, is

$$\mathbf{A}(\mathbf{x}) = -\frac{2\mu_0 \mu_r^{\mathrm{I}} \mu_B J}{r^2} \left\{ \int_0^r \mathcal{P}(r') r'^2 dr' \right\} \times \begin{pmatrix} 0 \\ \sin\eta \sin\phi \\ \sin\eta \cos\theta \cos\phi - \cos\eta \sin\theta \end{pmatrix}_{\hat{\mathbf{r}}, \hat{\boldsymbol{\theta}}, \hat{\boldsymbol{\phi}}}, \tag{5}$$

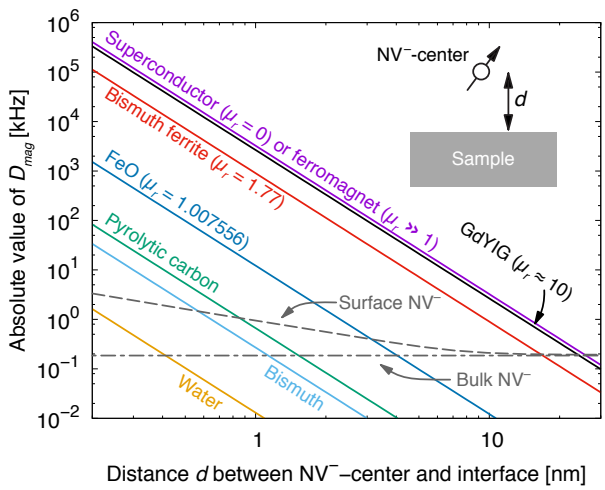

FIG. 3. The magnetic energy contribution $D_{\rm mag}$ to the fine structure constant as function of the distance d between the NV$^-$-center and the sample, for samples having different magnetic permeabilities. The grey lines indicate the measurable change in D for measurement time of 100s, reported for a bulk NV$^-$-center (dot-dash) and estimated for surface NV$^-$-centers (dash); see text for details. We took the low frequency values for μ_r and assumed the superconductor to be a perfect diamagnet (i.e. vanishing penetration depth). The μ_r of pyrolytic carbon, bismuth, and water are respectively 0.999590, 0.999834, and 0.999992.

for $r \leq R$, and the image current produces a vector potential

$$\widetilde{\mathbf{A}}(\mathbf{x}) = \frac{\mu_r^{\rm II} - \mu_r^{\rm I}}{\mu_r^{\rm II} + \mu_r^{\rm I}} \left\{ \frac{\mu_0 \mu_r^{\rm I} \mu_B J}{2\pi \left(4d^2 - 4rd\cos\theta + r^2\right)^{3/2}} \right\} \times \begin{pmatrix} -2d\sin\eta\sin\theta\sin\phi \\ (r - 2d\cos\theta)\sin\eta\sin\phi \\ (r\cos\theta - 2d)\sin\eta\cos\phi + r\cos\eta\sin\theta \end{pmatrix}_{\hat{\mathbf{r}},\hat{\boldsymbol{\theta}},\hat{\boldsymbol{\phi}}}, \quad (6)$$

for $z < d$. These vector potentials determine the spin's magnetic induction $\mathbf{B}(\mathbf{x}) = \nabla \times \mathbf{A}(\mathbf{x})$, see Fig. 2(b). The magnetic induction is either repelled from (drawn to) region II if $\mu_r^{\rm II} < \mu_r^{\rm I}$ ($\mu_r^{\rm II} > \mu_r^{\rm I}$), as the magnetization in region II is induced by the spin's magnetic field, and is either anti-parallel (diamagnetic) or parallel (paramagnetic) to the spin's magnetic field.

Using Eq. (2) the magnetic energy

$$E_{\rm mag} = \frac{16}{3}\mu_0 \mu_r^{\rm I} \mu_B^2 \pi \int_0^R \mathcal{P}(r)^2 r^2 dr + \left(\frac{\mu_r^{\rm II} - \mu_r^{\rm I}}{\mu_r^{\rm II} + \mu_r^{\rm I}}\right) \frac{\mu_0 \mu_r^{\rm I} \mu_B^2 J^2}{32\pi d^3} \left[3 + \cos 2\eta\right]. \quad (7)$$

The first term is the magnetic energy of the spin itself, and is inversely proportional to R^3 (for $\mathcal{P}(r) = \left[j_0(\pi r/R)\right]^2$, a spherical Bessel function of zeroth order). The magnetic self energy is experimentally inaccessible and goes to infinity for $R \to 0$, a well known problem in classical electrodynamics [20, 21]. The second term in Eq. (7) represents the change to the magnetic energy due to the presence of region II. These corrections are independent of $\mathcal{P}(r)$ due to the assumed spherical symmetry. The other dependencies of the magnetic energy are trivial to understand, after realizing that the change in magnetic energy depends on how much of the spin's magnetic induction penetrates region II. The magnitude of the angular variation of the magnetic energy for $d = 1$ nm is of the order of 10 neV (or 0.2 mK), which is extremely challenging to measure by spectroscopy. Also the resulting force $\mathbf{F} = -\nabla E_{\rm mag} \approx$ aN exerted on the scanning probe would be difficult to detect by atomic force microscopy. Instead, we will show that the magnetic energy can be probed using a coherent measurement of a NV$^-$-center's spin.

The ground state of a NV's spin $J = 1$ is effectively described using the Hamiltonian $\mathcal{H}_{\rm NV} = D_{\rm GS} J_z^2$, where $D_{\rm GS} \approx 2.87$ GHz is the fine structure constant due to the crystal field, and the z-direction is the NV-center's symmetry axis [19], see Fig. 1(a). To compare the NV$^-$-center spin with the spin considered in Fig. 2(a), it is convenient to orient the NV$^-$-center's symmetry axis perpendicular to the interface between the two regions. It has recently been demonstrated that such orientation can be realized deterministically in practice [22]. Analogous to the spin considered in Fig. 2(a), the NV$^-$-center's spin is placed in the superposition $|J_\eta\rangle = \cos^2\frac{\eta}{2}|+1\rangle + \frac{1}{2}\sqrt{2}\sin\eta|0\rangle + \sin^2\frac{\eta}{2}|-1\rangle$, such that the expectation value of the spin makes an angle η with respect to the z-axis. The energy of this state

$$\langle J_\eta|\mathcal{H}_{\rm NV}|J_\eta\rangle = \frac{D_{\rm GS}}{4}\left[3 + \cos 2\eta\right], \quad (8)$$

is identical to the angular dependence of the magnetic energy in Eq. (7). Therefore the effect of a nearby region with different magnetic permeability on the spin of a NV$^-$-center seems to effectively change its fine structure constant.

A fully quantum-mechanical treatment of the spin results in the magnetic energy Hamiltonian (see Supplemental Material [18])

$$\mathcal{H}_{\rm mag} = \left(\frac{\mu_r^{\rm II} - \mu_r^{\rm I}}{\mu_r^{\rm II} + \mu_r^{\rm I}}\right) \frac{\mu_0 \mu_r^{\rm I} \mu_B^2}{16\pi\hbar^2 d^3} J_z^2 = D_{\rm mag} J_z^2, \quad (9)$$

so that the NV$^-$-center effectively has $D = D_{\rm GS} + D_{\rm mag}$. Since the magnetization induced in region II depends on the spin and acts back on the spin itself, $\mathcal{H}_{\rm mag}$ depends on the spin squared. In the Supplemental Material [18] we show that $\mathcal{H}_{\rm mag}$ has a similar structure when $\mathcal{P}(\mathbf{x})$ has cylindrical symmetry and has its axial symmetry axis is perpendicular to the interface between regions I and II. We also calculated that cylindrical symmetry changes a NV$^-$-center's $D_{\rm mag}$ by $\leq 5\%$ from the spherical approx-

imation. Lowering the symmetry further to NV$^-$'s $C_{3,v}$-symmetry leads to additional small corrections, which we estimate to be less than 20% for an NV$^-$-center 1 nm away from the interface. Assuming a spherical $\mathcal{P}(\mathbf{x})$ is therefore a reasonable approximation. Note that in the classical limit $J \to \infty$ we get $\langle J_\eta | \mathcal{H}_{\rm mag} | J_\eta \rangle = E_{\rm mag}$, and there is no effect for $J = \frac{1}{2}$.

The following (briefly outlined) coherent measurement protocol can be used to sensitively measure D; more details can be found in Ref. [14]. The NV$^-$-center is first prepared in the $|J_z = 0\rangle$ state using a pulsed optical excitation, by making use of the spin-dependent decay from the excited state manifold to the ground state manifold [19]. The spin is then placed in a superposition of the $|J_z = 0\rangle$ and $|J_z = \pm 1\rangle$ states using a $\pi/2$ microwave pulse at frequency D. This superposition will acquire a phase $\exp(-iD\tau)$ after a free evolution time τ. By applying another $\pi/2$ microwave pulse to project the spin onto the $|J_z = 0\rangle$ state, the phase can be determined by optical measurement of the $|J_z = 0\rangle$ population; D follows from measuring the phase as function of τ most accurately through the use of a reference oscillator. The spin will experience decoherence during its free evolution, which can be mitigated using dynamic decoupling protocols, which can be designed to optimize the sensitivity at which D can be measured [14].

In Fig. 3 we show how $D_{\rm mag}$ depends both on the distance d between the NV$^-$-center and the sample, and on the relative magnetic permeability of the sample. Diamond itself has a very weak diamagnetic response, $\mu_r = 1 - 2.2 \times 10^{-5}$ [23], and has no free carriers. The NV$^-$-center is therefore in practice magnetically insensitive to its host, and $D_{\rm mag}$ is barely affected by the diamond's shape. Using a coherent measurement technique, D has been measured with a sensitivity of 1.85 kHz/$\sqrt{\rm Hz}$ [14]. Assuming a measurement time of 100s, changes in D of 0.2 kHz can therefore be detected for bulk NV$^-$-center. From Fig. 3 it appears possible to detect both paramagnetic and diamagnetic substances if the NV$^-$-center is a few nm away from the sample. Such small distances are conventional in scanning probe microscopy [24], and have been achieved in conventional NV$^-$-center magnetometry [25]. Recent studies showed that the proximity of the surface lowers the NV-center's T_2 coherence time due to a surface electronic spin bath and/or surface phonon-related mechanism [26–28]. This increases the minimal detectable change in D by a factor $\sqrt{T_2^{\rm bulk}/T_2^{\rm surface}}$ [14]. Based on the experimental data of Ref. [28], we roughly estimated the dependence of this ratio on d. We included in Fig. 3 both the minimal detectable change in D estimated for near-surface and reported for bulk NV$^-$-centers for a measurement time of 100s. Increasing T_2 (potentially by mitigating the surface phenomena by surface passivation), improving sensing schemes, or extending the measurement time would push the minimal detectable change in D down.

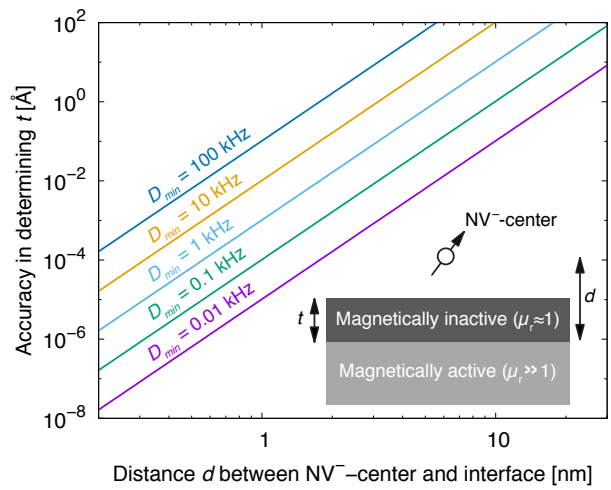

FIG. 4. The accuracy at which the thickness t of a magnetically dead layer (μ_r is about 1) can be determined, as function of the distance d between the NV$^-$-center and the magnetically active region ($\mu_r \gg 1$), for different minimal detectable changes $D_{\rm min}$. Based on Ref. 14, $D_{\rm min} = 0.2$ kHz for a bulk NV$^-$-center and a measurement time of 100s. See Fig. 3 and its discussion in the text for estimated $D_{\rm min}$ close to the surface.

Our analysis is not limited to NV$^-$-centers; any spin close to a region with different magnetic permeability will experience an orientation dependent magnetic energy, which affects its dynamics. Therefore the spins of other promising color centers [29], notably the divacancy in SiC, could also be used to detect magnetic properties of nearby materials. Such systems would preferably have a smaller fine structure constant $D_{\rm GS}$, since in the proposed measurement scheme the NV$^-$-center's spin is precessing at that frequency. Although this does not impede the effect of the magnetic energy on the fine structure constant, it does set the frequency at which the magnetic properties of the sample are probed; lowering this frequency would be favorable. Alternatively, different measurement schemes could be developed, which remove the necessity of the spin precessing at such frequencies.

As an example of the added value of the proposed magnetic energy based magnetometry, we suggest to use this technique to measure the thickness t of magnetically dead layers [17]. A common problem in magnetic multilayered materials, such as magnetic tunnel junctions [30], is the magnetic inactivity of the top surface layer of the structure, see inset of Fig. 4. We can make use of the strong distance dependence of the magnetic energy ($E_{\rm mag} \propto d^{-3}$) to sensitively determine the distance d between the NV$^-$-center and the boundary of the magnetically active material. As the separation between the NV$^-$-center and the physical boundary of the sample is known through calibration, the thickness t of the magnetically inactive material can be determined with high

precision. Figure 4 predicts that this can be achieved with remarkable accuracy.

We propose a method to sense the magnetic properties of materials based on the magnetic energy of a nearby spin. This method inverts the conventional scheme of scanning probe magnetometers, making it possible to sense materials which have no natural magnetic field external to their volume. This scheme can be applied to NV^--centers and, using realistic assumptions, we predict it should be possible to detect both para- and diamagnetic materials. Future theoretical work towards implementing different color centers or different measurement schemes could lower the frequency at which the magnetic properties are probed and improve the predicted sensitivity.

The authors acknowledge support from an AFOSR MURI.

* j.v.bree@tue.nl
† michael_flatte@mailaps.org

[1] I. I. Rabi, J. R. Zacharias, S. Millman, and P. Kusch, Phys. Rev. **53**, 318 (1938).
[2] R. C. Jaklevic, J. Lambe, A. H. Silver, and J. E. Mercereau, Phys. Rev. Lett. **12**, 159 (1964).
[3] F. W. Wehrli, Physics Today **45**, 34 (1992).
[4] G. Balasubramanian, I. Y. Chan, R. Kolesov, M. Al-Hmoud, J. Tisler, C. Shin, C. Kim, A. Wojcik, P. R. Hemmer, A. Krueger, T. Hanke, A. Leitenstorfer, R. Bratschitsch, F. Jelezko, and J. Wrachtrup, Nature **455**, 648 (2008).
[5] L. Ciobanu, D. Seeber, and C. Pennington, Journal of Magnetic Resonance **158**, 178 (2002).
[6] P. Glover and S. P. Mansfield, Reports on Progress in Physics **65**, 1489 (2002).
[7] Y. Martin and H. K. Wickramasinghe, Applied Physics Letters **50**, 1455 (1987).
[8] A. M. Chang, H. D. Hallen, L. Harriott, H. F. Hess, H. L. Kao, J. Kwo, R. E. Miller, R. Wolfe, J. van der Ziel, and T. Y. Chang, Applied Physics Letters **61**, 1974 (1992).
[9] C. L. Degen, M. Poggio, H. J. Mamin, C. T. Rettner, and D. Rugar, Proceedings of the National Academy of Sciences **106**, 1313 (2009).
[10] S. Hong, M. S. Grinolds, L. M. Pham, D. Le Sage, L. Luan, R. L. Walsworth, and A. Yacoby, MRS Bulletin **38**, 155 (2013).
[11] E. van Oort, N. B. Manson, and M. Glasbeek, Journal of Physics C: Solid State Physics **21**, 4385 (1988).
[12] L. Childress, M. V. G. Dutt, J. M. Taylor, A. S. Zibrov, F. Jelezko, J. Wrachtrup, P. R. Hemmer, and M. D. Lukin, Science **314**, 281 (2006).
[13] J. R. Maze, P. L. Stanwix, J. S. Hodges, S. Hong, J. M. Taylor, P. Cappellaro, L. Jiang, M. V. G. Dutt, E. Togan, A. S. Zibrov, A. Yacoby, R. L. Walsworth, and M. D. Lukin, Nature **455**, 644 (2008).
[14] D. M. Toyli, C. F. de las Casas, D. J. Christle, V. V. Dobrovitski, and D. D. Awschalom, Proceedings of the National Academy of Sciences **110**, 8417 (2013).
[15] G. Kucsko, P. C. Maurer, N. Y. Yao, M. Kubo, H. J. Noh, P. K. Lo, H. Park, and M. D. Lukin, Nature **500**, 54 (2013).
[16] P. Neumann, I. Jakobi, F. Dolde, C. Burk, R. Reuter, G. Waldherr, J. Honert, T. Wolf, A. Brunner, J. H. Shim, D. Suter, H. Sumiya, J. Isoya, and J. Wrachtrup, Nano Letters **13**, 2738 (2013).
[17] J. Z. Sun, D. W. Abraham, R. A. Rao, and C. B. Eom, Applied Physics Letters **74**, 3017 (1999).
[18] See Supplemental Material at [url] for the derivation of the spin density of a N-particle state [validating Eq. (1)], and for the derivation of the magnetic energy Hamiltonian treating the spin fully quantum-mechanically and assuming a spherically or cylindrically symmetric probability density. The Supplemental Material includes Refs. [31–33].
[19] M. W. Doherty, N. B. Manson, P. Delaney, F. Jelezko, J. Wrachtrup, and L. C. L. Hollenberg, Physics Reports **528**, 1 (2013).
[20] J. D. Jackson, *Classical Electrodynamics*, 3rd ed. (Wiley, New York, 1998).
[21] L. D. Landau and E. M. Lifshitz, *The Classical Theory of Fields*, 3rd ed., Landau and Lifshitz Course of Theoretical Physics, Vol. 2 (Pergamon Press, 1971).
[22] J. Michl, T. Teraji, S. Zaiser, I. Jakobi, G. Waldherr, F. Dolde, P. Neumann, M. W. Doherty, N. B. Manson, J. Isoya, and J. Wrachtrup, Applied Physics Letters **104**, 102407 (2014).
[23] W. M. Haynes, *Handbook of Chemistry and Physics* (CRC, 2015).
[24] Y. Seo and W. Jhe, Reports on Progress in Physics **71**, 016101 (2008).
[25] M. Loretz, S. Pezzagna, J. Meijer, and C. L. Degen, Applied Physics Letters **104**, 033102 (2014).
[26] T. Rosskopf, A. Dussaux, K. Ohashi, M. Loretz, R. Schirhagl, H. Watanabe, S. Shikata, K. M. Itoh, and C. L. Degen, Phys. Rev. Lett. **112**, 147602 (2014).
[27] B. A. Myers, A. Das, M. C. Dartiailh, K. Ohno, D. D. Awschalom, and A. C. Bleszynski Jayich, Phys. Rev. Lett. **113**, 027602 (2014).
[28] Y. Romach, C. Müller, T. Unden, L. J. Rogers, T. Isoda, K. M. Itoh, M. Markham, A. Stacey, J. Meijer, S. Pezzagna, B. Naydenov, L. P. McGuinness, N. Bar-Gill, and F. Jelezko, Phys. Rev. Lett. **114**, 017601 (2015).
[29] L. Gordon, J. R. Weber, J. B. Varley, A. Janotti, D. D. Awschalom, and C. G. Van de Walle, MRS Bulletin **38**, 802 (2013).
[30] S. Ikeda, K. Miura, H. Yamamoto, K. Mizunuma, H. D. Gan, M. Endo, S. Kanai, J. Hayakawa, F. Matsukura, and H. Ohno, Nature Materials **9**, 721 (2010).
[31] F. Schwabl, *Advanced quantum mechanics* (Springer, 2004).
[32] J. D. Bjorken and S. D. Drell, *Relativistic quantum fields* (McGraw-Hill, 1965).
[33] A. Gali, M. Fyta, and E. Kaxiras, Phys. Rev. B **77**, 155206 (2008).